EARTHQUAKE PERFORMANCE OF HIGH-STRENGTH CONCRETE STRUCTURAL WALLS WITH BOUNDARY ELEMENTS

YUN, hyun-do[1], CHOI, chang-sik[2] and LEE, li-hyung[3]

SUMMARY

This paper addresses the behavior and strength of structural walls with a concrete compressive strength exceeding 69 MPa. This information also enhances the current database for improvement of design recommendations. The objectives of this investigation are to study the effect of axial-load ratio on seismic behavior of high-strength concrete flexural walls. An analysis has been carried out in order to assess the contribution of deformation components, i.e. flexural, diagonal shear, and sliding shear on total displacement. The results from the analysis are then utilized to evaluate the prevailing inelastic deformation mode in each of wall. Moment-curvature characteristics, ductility and damage index are quantified and discussed in relation with axial stress levels. Experimental results show that axial-load ratio have a significant effect on the flexural strength, failure mode, deformation characteristics and ductility of high-strength concrete structural walls.

INTRODUCTION

In the seismic design of buildings, reinforced concrete structural walls, or shear walls, act as major earthquake resisting members. Structural walls provide an efficient bracing system and offer great potential for lateral load resistance. The properties of these seismic shear walls dominate the response of the buildings, and therefore, it is important to evaluate the seismic response of the walls appropriately. Recently, a high-strength concrete with a compressive strength in range of 60 to 100 MPa has successfully been utilized in columns and core-walls of multi-story buildings. However, very few experimental works has been reported with reference to the behavior of high-strength concrete structural walls.

Over the past three decades, major advances have been made in the understanding of the behavior of reinforced concrete structural walls, particularly with regard to the role of the variables improving seismic

[1] Associate Professor, Div. of Architecture, Chungnam National Univesity, Daejeon, Korea
  Email: wiseroad@cnu.ac.kr
[2] Associate Professor, Dept. of Architectural Engineering, Daejin Univesity, Kyunggido, Korea
  Email: cschoi@daejin.ac.kr
[3] Professor, School of Architecture, Hanyang University, Seoul, Korea
  Email: leelh@hanyang.ac.kr

performance.[1] However, little experimental work has been done to assess the behavior of reinforced concrete shear walls subjected to high axial load, partly because of the difficulty of applying high axial loads to slender shear walls due to the inherent out-of-plane wall instability problem. Lefas (1988)[2] studied the effect of axial load on strength, stiffness, and deformation characteristics of rectangular walls under a constant axial load and a monotonically increasing horizontal load. As a part a five national research (New-RC) project in Japan, a total of twenty-one high strength, 60 MPa to 120 MPa, concrete shear walls were tested and results were compiled by Kabeyasawa et al (1993)[3]. The Gupta and Rangan (1998)[4] carried out tests on eight flanged wall specimens subjected to monotonic loading. Zhang and Wang (2000)[5] investigated the influence of axial-load ratio and shear compression ratio on the behavior of rectangular shear walls. While little research has been carried out on the framed walls under high gravity load and seismic action, high-strength concrete framed walls are becoming more frequently used as the lateral resisting elements in wide-bay high-rise buildings. This investigation is an exploratory phase of an experimental program of high-strength concrete framed walls subject to the combined action of constant high axial load and reversed cyclic horizontal loading.

EXPERIMENTAL PROGRAM

Test specimen

The scope of the experiment was limited to tests on isolated wall specimens. The test specimens were subjected to constant axial compressive force and reversed cyclic horizontal loading. All the specimens were designed based on the philosophy that the lateral load capacity was controlled by flexure and therefore, the undesirable premature shear failure during the experiment would be prevented. The overall dimensions of the test specimens were kept constant.

Three isolated flexural walls, as shown in Fig. 1, were constructed and tested in this investigation. The dimensions of the specimens correspond to one-third the dimensions of the prototype. To scale down the prototype structure to the specimens, two independent scale factors were chosen for stress and length, respectively; all remaining scale factors were either equal to unity or were functions of two factors. Each wall was tested under combined action of constant axial load and horizontal load reversals. All three wall specimens, HW1 to HW3, had boundary elements. Boundary element transverse reinforcement, 6mm diameter hoops spaced at about 40mm, was selected in a way such that adequate confinement to core concrete would be provided, and longitudinal reinforcement buckling in the post-yielding stage would also be prevented. The geometry, dimensions, amount and arrangement of boundary elements of walls were identical for all three specimens. The main flexural reinforcement of each boundary element consisted of eight 10mm diameter high-tensile deformed steel bar arranged in a rectangular manner.

All the specimens had the same geometry and were monolithically connected to the top and foundation beam. A heavily reinforced top beam(1.50m long×300mm deep×300mm wide) functioned as both a uniform load transfer through which axial and horizontal loads were applied to the walls and as a cage for anchorage of the vertical bars. The foundation beam(1.50m long×400mm deep×500mm wide) was utilized to clamp the specimens to the laboratory floor, simulating a rigid foundation. A summary of the experimental program is presented in Table 1. The overall geometry and dimensions of the wall specimens and reinforcement details are shown in Fig. 1.

All the specimens were designed using 0.55% horizontal and 0.55% vertical web reinforcement ratios. Vertical reinforcement consisted of 7 pairs of 6mm diameter high-tensile round steel bar, uniformly placed in two layers. Uniformly distributed horizontal web steel consisted of two layers of 6mm diameter high-tensile round steel bar. The bars were spaced at 120mm along the full height of the wall. The horizontal bars were anchored into the core of each boundary element using 90-degree hooks.

All reinforcing bars were provided with adequate anchorage lengths at their ends. This was achieved by providing cogs at the ends of the bars. All closed ties were terminated with 135-degree hooks. In all

specimens, the clear concrete cover to reinforcement was 20mm. Additional horizontal reinforcement, four 10mm diameter deformed bars, was arranged at each floor slab level.

Material properties
Commercial ready-mixed concrete with replacement of 7.8 %(by weight) cement by silica fume was used and was made using a selected ASTM Type I Portland cement. A high-range water reducer (superplasticizer) and water-reducing retarder were added to the mix to improve workability. The specified 28-day compressive strength of the mix was 68.7MPa. The maximum size of aggregate was 15mm in order to ensure good compaction of concrete in the test specimen. The slump of the concrete was 150mm. For each batch, 100×200mm cylinders were made to measure the compressive strength and the splitting tensile strength of concrete. The measured concrete strength and elastic modulus were tested by the ASTM standard test method. The compressive strength and the splitting tensile strength on the day of the wall test are given in Table 2.

The reinforcing steel for all the walls was obtained from one batch of steel for each bar diameter. Three samples were taken and tested from each diameter of reinforcing used. Tension tests were conducted on full-size bar samples in accordance with ASTM A370 to determine yield strength, ultimate strength, and total elongation. Physical properties of reinforcing steel are given in Table 3. The test wall specimens were monolithically connected to foundation beams and cast horizontally in timber molds.

Testing apparatus
The testing apparatus is shown in Fig. 2. The wall footing is rigidly connected to the strong floor using eight 32mm diameter high-tension bolts. A 980kN MTS hydraulic actuator attached to the reaction frame was used to apply a horizontal force to the load transfer assembly mounted on the top of the wall. To ensure out of plane stability and represent the diaphragm effect of a floor slab, the wall is laterally guided by low friction sliding ball bearings at the levels of the first and second floor. Axial load was provided with a 980kN MTS hydraulic actuator on the top of the load transfer assembly and maintained concentric to the test wall at all stages of loading.

The data acquisition system consisted of thirty-six internal control and recording channels. Instrumentation was provided to measure loads, displacement, and strains at critical locations. Lateral and axial load were measured using load cells capable of maintaining linearity up to 980kN. The load cells were calibrated before and after each test in a test machine. As shown in Fig. 3, the displacements of each specimen were measured using Linear Variable Differential Transducers (LVDTs). Two LVDTs were installed at the top of the specimen to monitor the top displacement. The horizontal displacement profile of each specimen was measured using LVDT at each storey level (at three locations over the wall height). One LVDT was installed at a distance of 100mm from the wall base to measure the sliding of the base. Twelve LVDTs were installed close to the boundary elements to measure the curvatures along the height of walls to obtain the flexural deflection. Steel strain gages were also provided on numerous hoops and cross ties within the boundary elements and on horizontal and vertical reinforcement within the web. The foregoing system of measurements made it possible to estimate the flexural, shear, and sliding components of the wall deformation.

Testing procedure
A constant axial load was first applied through a spread beam at the centers of the boundary elements of walls. HW1 to HW3 were subjected to three levels of axial-load ratio corresponded to 0.24, 0.12, and 0.00 of the uniaxial compressive strength of the wall cross-section that is equal to $0.97f_cA_g$. These levels of axial load might be considered representative of the amount at the base of a single story, medium-rise, and high-rise building, respectively. During each test, the displacement at the top of the wall was controlled.

A reverse cyclic loading was applied slowly to the top of the specimens. Initially, the test specimen was exercised by applying 49kN horizontal load in order to ensure that all systems were working. The initial

load was then released and zero reading was taken. The walls were cycled three times at each of the incrementally increasing deflection level until failure. The deflection increments were based on yield deflection. The yield deflection was determined by drawing a straight line from the origin through the first yield load and its intersection with a horizontal line drawn at calculated ultimate load level. The first yield load was obtained experimentally when the strain gages on the extreme tension reinforcement at the boundary elements yielded.

EXPERIMENTAL RESULTS

Crack process and failure mode
Flexural cracks initially appeared at the base of the boundary elements in the tensile zone during the first elastic loading, and the cracks propagated from the wall boundary elements toward the center and from the bottom upwards. These cracks were initially horizontal and confined within the length of the boundary elements, but as the loading increased, they became slightly inclined downwards and extended into the web (see Fig. 4). Eventually, these cracks formed a diagonal cracking pattern in the web. The inclination increased along the wall height. At the boundary elements, the density of the cracks increased, while in the web the number of main cracks was limited to about four or five on each side. In the lower part of the wall, flexural cracks originating from one edge were intersected by inclined shear or flexural-shear cracks originating from the opposite edge, resulting in a characteristic criss-cross pattern (see Fig. 5). With cycling to increased deformations, the rhomboidal pieces of concrete between the intersecting cracks gradually deteriorated and spalling of cover concrete occurred. The spalling zone extended further upwards in the case of specimen HW3, which was subjected to horizontal load without axial force (see Fig. 6(c)).
Significant loss of strength, leading to failure, was observed when concrete started to deteriorate in the most heavily stressed parts of the boundary elements. The web, hoops, and horizontal bars began to lose support and move away from each other as buckling and kinking of the longitudinal bars occurred. The effects of the axial stress ratio on the cracking pattern and failure mode of the specimens can be seen in Fig. 6. Because wall behavior was controlled by flexure, the cracking process was similar for all specimens (see Fig. 4 and 5).
Observed cracking patterns at yielding, ductility of 3 and failure are shown in Fig. 4, 5 and 6. High axial stress ratios restrained the development of major inclined cracks in the web. This is because increased axial force will reduce the principal tensile stress in the web portion of the wall. The presence of higher levels of constant axial force led to even less extensive crack formation. Fewer flexural cracks were formed at the tensile edge of the wall and diagonal cracking covered less of the web of the wall. Nevertheless, higher axial force levels only managed to delay but not prevent the extension of the inclined crack within the lower compressive edge of the boundary elements.

Load-displacement response
Base shear force versus top displacement hysteresis loops for all specimens are shown in Fig. 7. In the figure, the well-known characteristics of reinforced concrete members subjected to cyclic loading, such as unloading and reloading stiffness reduction as the cyclic displacement amplitude increases and pinching of hysteresis loops can be clearly seen. Some ductility was observed for specimens subjected to large axial forces (see Fig. 7(a) through (c)). As axial force was increased, load-displacement curves showed an S shape hysteresis loop with small residual displacements.
The strength of all specimens except HW3 increased due to the presence of the compression axial force, but ductility was slightly inferior to that of HW3. Significant strength degradation occurred at a displacement of 52mm (2.65 % drift) following extensive concrete crushing and reinforcement buckling at the boundary elements; further cycling led to eventual fracture of some buckled bars. Hence, inelastic performance of high-strength concrete structural walls represented stable behavior in flexural yielding and

maintaining horizontal load-carrying capacity.

Strength, stiffness and energy dissipation characteristics

Predicted results of ACI Building Code[6] and Architectural Institution of Japan (AIJ) Guideline[7] are summarized in Table 4 and compared with the experimental values. Predicted flexural strength of the specimen HW3, which was not subjected to axial force, was almost the same as the observed load-carrying capacity of specimen. For the specimens HW1 and HW2 with axial stress ratio of 0.24 and 0.12 respectively, the measured strengths of these specimens were larger than their predicted strengths by approximately 13%. This can be attributed to the enhanced concrete strength due to confinement from surrounding concrete. The ACI 318-02 and AIJ Guideline seem to be slightly conservative in this respect.

The reduction of strength and stiffness of reinforced concrete, especially high-strength concrete, members subjected to cyclic loading are significant for structures in seismic areas. Therefore, seismic resistant members with significant degradation of strength and stiffness due to the imposition of severe cyclic loading must be avoided in seismic design. Fig. 7 indicates that the horizontal load-carrying capacity of a wall is dependent on the level of axial force. Table 4 also indicates that the strengths of the walls with axial stress ratio of 0.12 and 0.24 was greater than that of the wall subjected to only horizontal load by about 60.2% and 88.8%, respectively. The maximum shear load for each displacement step, V_i, is plotted as a fraction of the maximum shear strength, V_{max}. The data are plotted versus the displacement ductility ratio (δ_i/δ_y) shown in Fig. 8 for all walls.

The stiffness characteristics of high-strength concrete flexural walls, which are a function of the slopes of the load-deformation curves, were influenced considerably by the effects of the level of axial force. Stiffness characteristics of structural walls were dominated by a severe loss of stiffness during and after yield. A principal cause for the loss of stiffness in walls was the diagonal shear crack and crushing of wall web concrete. All of the specimens showed an increase in secant stiffness values as the applied level of constant vertical stress increased. In early stages, the secant stiffness of HW1 was higher than that for HW2 and HW3. However, with increasing loading cycles, the variation of secant stiffness for HW3 was more stable than that of HW1 and HW2. It can be concluded that axial force has a detrimental effect on stiffness variation in the post-yielding stage of flexural wall deformation. Stiffness decay as noted by the relation between the ratio k_i/k_y and displacement ductility is shown in Fig. 9, where k_i is equal to the secant stiffness values corresponding to the first half-cycle in each stage.

Energy dissipation under cyclic loading was defined as the area enclosed by the base shear force versus top displacement hysteretic loops shown in Fig. 6. The amount of energy dissipated prior to first significant cracking of the wall was relatively small, but increased greatly once this level was exceeded. It is obvious that energy dissipation capacity rose with the increase of axial stress ratio. The relationship between normalized energy dissipated and displacement ductility is summarized in Fig. 10. The normalized energy dissipated was defined as the energy dissipated in half hysteresis loop corresponding to positive load direction divided by $0.5V_y\delta_y$, where V_y and δ_y are the yielding load and yielding displacement, respectively. As noted by comparing curves for specimens HW1 and HW3, high axial force had a detrimental effect on energy dissipation behavior.

Total energy applied to the wall during virgin loading can be separated into three components, namely, the recoverable energy, damping energy, and the damage energy. The energy dissipated by a wall is the sum of the damage energy and the damping energy. Another way of presenting the energy dissipated per cycle during a cyclic loading test is by using the concept of equivalent viscous damping. This term has been used by investigators to correlate hysteretic energy dissipation to the standard concept of structural damping used for linear systems. Generally, measurements of dynamic response of actual structures in the elastic range close to the yield strength indicate that equivalent viscous damping levels of 5% to 7% for reinforced concrete are appropriate.[8] In the elastic range close to yield strength, the equivalent viscous damping level of high-strength concrete flexural walls tested was approximately 5%.

Components of displacement
An attempt has been made to assess the contribution of each deformation component on total displacement of the wall specimens. The deformation components include flexural, shear in the web, and the horizontal sliding shear deformation at the base. The sliding shear deformation component was measured with LVDTs attached between the footing and the wall panel. The flexural component was calculated as the sum of the average measured layer curvature multiplied by each layer height. The shear component was then evaluated by the measured top displacement subtracted by the above two components. Fig. 11 displays a typical example of hysteresis loops for HW1 and HW3 specimens with and without axial force, respectively.

The contribution of each deformation mode to the total displacement of wall specimens is shown in Fig. 12 for various ductility levels. It is clear from the figure that the relative contribution of each component is significantly varying with the ductility level. Initially, shear deformation dominated the response. However, after yielding, flexure deformation governed the response, being a major contributor to the total displacement. For the high axial-load ratio wall specimen HW1, shear deformation reached up to 64% of the total displacement at yielding. However, as the ductility is increased (2 or more), flexural deformation is more pronounced, being approximately 55% of the total displacement. It is noted that the sliding shear deformation component was minor, being 0.4% and 3.1% of the total displacement at yielding and at close to failure, respectively. Whereas the deformation modes of the HW2 specimen were similar to those of HW1 shown in Fig. 12(a), the contribution of sliding shear deformation was considerable (approximately 19% of the total displacement at ductility of 9) for the HW3 specimen without axial force.

For most of walls, the contribution of shear deformation was significantly lower than that of flexural deformation. As expected, compressive axial played a significant role on the reduction of base sliding and shear deformation, respectively.

Ductility
The term ductility defines the ability of a structure and selected structural components to deform beyond elastic limits without excessive strength or stiffness degradation. The most convenient quantity to evaluate either the ductility imposed on a structure by an earthquake or the structure's capacity to develop ductility is displacement ductility as Equation (1).

$$\mu_\delta \;=\; \frac{\delta_u}{\delta_y} \;\text{(1)}$$

Where, δ_y is top displacement at yielding (as the point of initiation of a pronounced non-linearity of the horizontal force versus the horizontal displacement curves); δ_u is the displacement at the point when the shear resistance level decayed to 85% of the observed maximum strength. The δ_u, displacement at 85% of the maximum horizontal force with the descending branch of the envelope of the hysteresis loop are taken as these at failure. This definition is in agreement with the 15% force response degradation of reinforced concrete elements acceptable by Eurocode 8.[11]

Table 5 and Fig. 13(a) show the effect of the two parameters investigated, namely the axial-load and the horizontal web reinforcement ratio, on ductility of high-strength concrete structural walls. In fact, by comparing the displacement ductility values for HW1, HW2, and HW3, which had the same horizontal reinforcement ratio but a different normalized axial-load ratio (equal to 0.24, 0.12, and 0.00 respectively), one may observe that for this axial load increase, the ductility decreased from 13.69 to 11.93 (13% reduction).

Damage indexes
Many authors have established a set of damage indexes to ascertain the residual capacity of structures. A wide array of parameters may be used, such as number of cycles, stiffness, and ductility. When reverse loads are applied, however, the importance of energy dissipation is readily apparent. The energy indicator proposed by Darwin and Nmai[12] provides an assessment of the dissipative capacity compared with the

elastic energy injected at peak load. This measurement has been related to the hysteretic area of cycle i, E_i normalized to the elastic energy $F_{max}\delta_{Fmax}$. The iteration on all cycles yields the total normalized cyclic energy, as follows

$$E_n = \frac{\sum E_i}{F_{max}\delta_{F\,max}} \quad (2)$$

This indicator has been modified by Ehsani and Wright[13] through introducing a damage index combining the cyclic dissipated energy, the stiffness degradation and the deformation capacity

$$W_i = \frac{\sum E_i}{F_{max}\delta_{F\,max}} \left(\frac{k_i}{k_y}\right)\left(\frac{\delta_i}{\delta_y}\right)^2 \quad (3)$$

Where, F_{max} is peak load; δ_{Fmax} and δ_i are deflection at the peak and maximal deflection of cycle i, respectively; E_i is dissipated energy calculated from the area of cycle i; and k_y and k_i are secant stiffness at the yielding and in cycle i, respectively.

To evaluate the effect of axial load in boundary element and transverse web reinforcement on the seismic resistance of high-strength concrete structural walls, two comparisons in damage index, E_n and W_i, were made between specimens and reported in Table 5. As axial stress in boundary elements increases, damage index reduced significantly. Therefore, while axial stress increases the horizontal load carrying capacity and secant stiffness, it improves the seismic resistance of high-strength reinforced concrete structural walls inefficiently.

CONCLUSIONS

The following conclusions are drawn based on the results of tests of high-strength concrete flexural walls:

1. Testing of high-strength concrete structural walls subjected to high axial stresses, up to $0.24f'_c$, shows that it is possible to ensure a predominantly ductile performance by promoting flexural yielding of the vertical reinforcement. Thus, in this respect, the behavior of high strength concrete is not significantly different from that of normal strength concrete.

2. The axial-load ratio had an important effect on the failure mode, hysteresis loop, stiffness, deformation characteristics and ductility of the high-strength concrete flexural walls. High-strength concrete flexural walls initially subjected to high level of axial stress, $0.24f'_c$, load showed an 89% enhancement in horizontal load capacity compared with the capacity of wall not subjected to axial load.

3. Higher depths of neutral axis were observed with increasing levels of axial compressive load applied to the wall specimen. HW1 and HW2 specimen, subjected to axial load, failed in a predominantly flexural mode, characterized by the concrete crushing and reinforcement buckling at the lower compressive zone of the boundary elements. The failure region, plastic hinge zone, was more extensive with axial load increasing. Web concrete crushing was observed for HW3 specimen.

4. The predicted strengths from ACI 318-02 Building Code and AIJ Guideline underestimated the measured load-carrying capacities of the high-strength concrete flexural walls tested. ACI and AIJ formulas seem slightly conservative based on the experiment results.

REFERENCES

1. Paulay, T. A., "Design of Ductile Reinforced Concrete Structural Walls for Earthquake Resistance," Earthquake Spectra, V.2, No. 4, 1986, pp. 783~823.

2. Lefas, I., "Behaviour of Reinforced Concrete Structural Walls and Its Implication for Ultimate Limit State, Design," PhD Thesis, University of London, 1988.

3. Kabeyasawa, T.; and Hiraishi, H., "Test and Analyses of High-Strength Reinforced Concrete Shear Walls in Japan," ACI SP 176-13, 1993, pp. 281~310.

4. Gupta, A.; and Rangan, B. V., "HSC Structural Walls," ACI Structural Journal, Vol. 95, No. 2, Mar.-Apr., 1998, pp. 194~204.

5. Zhang, Y. F.; Wang, Z. H., "Seismic Behavior of Reinforced Concrete Shear Walls Subjected to High Axial Loading," ACI Structural Journal, Vol. 97, No. 5, Sept.-Oct., 2000, pp. 739~750.

6. ACI Committee 318, "Building Code Requirements for Structural Concrete (ACI318-02) and Commentary (ACI318R-02)," American Concrete Institute, Michigan, 2002.

7. Architectural Institute of Japan (AIJ), "AIJ Structural Design Guidelines for Reinforced Concrete Buildings Based on Ultimate Strength Concept," AIJ, Tokyo, 1994.

8. Paulay, T. A.; and Priestley, M. J. N., "Seismic Design of Reinforced Concrete and Masonry Buildings," John Wiley & Sons, Inc., 1992, 744 pp.

9. Salim Razvi; and Murat Saatcioglu, "Confinement Model for High-Strength Concrete," ASCE, Vol. 125, No. 3, 1999, March, pp. 281~289.

10. Gupta A.K.; and Maestrini S.R., "Tension Stiffness Model for Reinforced Concrete Bars," Journal of Structural Engineering ASCE, Vol. 116, No. 3, 1990, pp. 769~790.

11. Eurocode 8, "Design Provisions for Earthquake Resistance of Structures," ENV 1998.1, Brussels, 1994.

12. Darwin, D.; and Nmai, C. K., "Energy Dissipation in RC Beams under Cyclic Load," Journal of Structural Engineering, ASCE. Vol. 112, No. 8, 1986, pp. 1829~1846.

13. Ehsani, M. R.; and Wright, J. K., "Confinement Steel Requirements for Connections in Ductile Frames," Journal of The Structural Division, ASCE, Vol. 116, No. 3, 1990, pp.751~767.

Table 1. Details of test specimens

Wall specimen	Axial-load ratio	Storey beam reinforcement ratio(%)	Wall			Boundary element		
			$W \times H \times T$ (m × m × mm)	ρ_v (%)	ρ_h (%)	$B \times D$ (mm×mm)	ρ_f (%)	ρ_s (%)
HW1	0.24	1.11	$1.2 \times 2.0 \times 85$	0.55	0.55	180×180	1.75	0.78
HW2	0.12	1.11	$1.2 \times 2.0 \times 85$	0.55	0.55	180×180	1.75	0.78
HW3	0.00	1.11	$1.2 \times 2.0 \times 85$	0.55	0.55	180×180	1.75	0.78

Table 2. Average concrete compressive strengths

Compressive strength(MPa)				Slump (mm)	Elastic modulus (MPa)	Poisson's ratio
5-day	7-day	28-day	90-day[*]			
42	63	65	69	150	33,150	0.11

[*] At the time of testing

Table 3. Properties of reinforcement bars

Type	Yield strength f_{sy}, (MPa)	Ultimate strength f_{su}, (MPa)
10mm diameter deformed bar	413.9	664.0
6mm diameter round bar	571.8	636.5

Table 4. Correlation of test and predicted strengths   (Unit : kN)

Specimen	ACI 318-02[6]						AIJ Guideline[7]			Experimental results
	Flexural strength		Shear strength				Flexural strength		Shear strength	
	V_y	V_u	V_s	$V_c + V_s$	V_n	Upper limit	V_y	V_u	V_q	
HW1	332.7	387.0	256.0	537.5	449.6	677.2	316.1	383.7	546.7	442.0
HW2	272.4	331.5	256.0	475.9	449.6	677.2	355.7	293.5	513.3	375.0
HW3	173.3	241.2	256.0	395.4	449.6	677.2	103.7	161.5	469.6	234.1

Table 5. Measured displacement response, ductility factor, and damage index

Wall specimen	Displacement (mm)		Displacement ductility (μ_δ)	Normalized energy index (E_n)	Work index (W_i)
	δ_y	δ_u			
HW1	4.30	24.90	11.93	253.0	1538.20
HW2	4.08	27.61	12.86	346.6	2413.27
HW3	3.24	30.99	13.69	417.1	2793.80
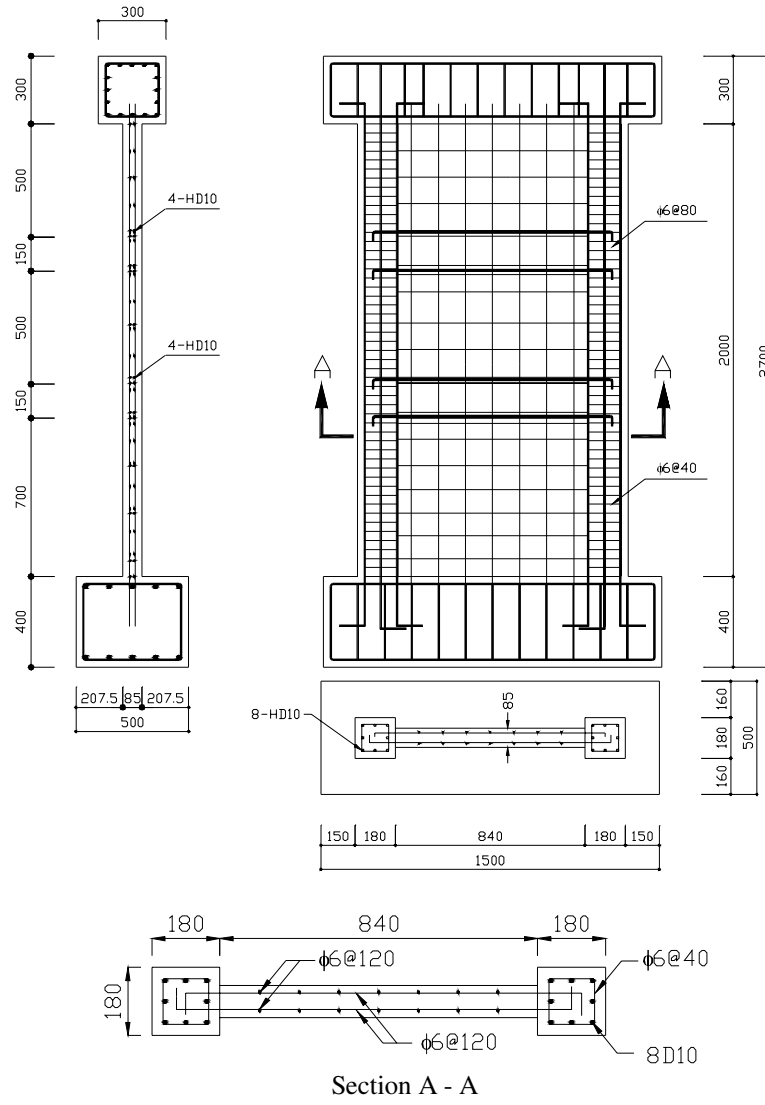
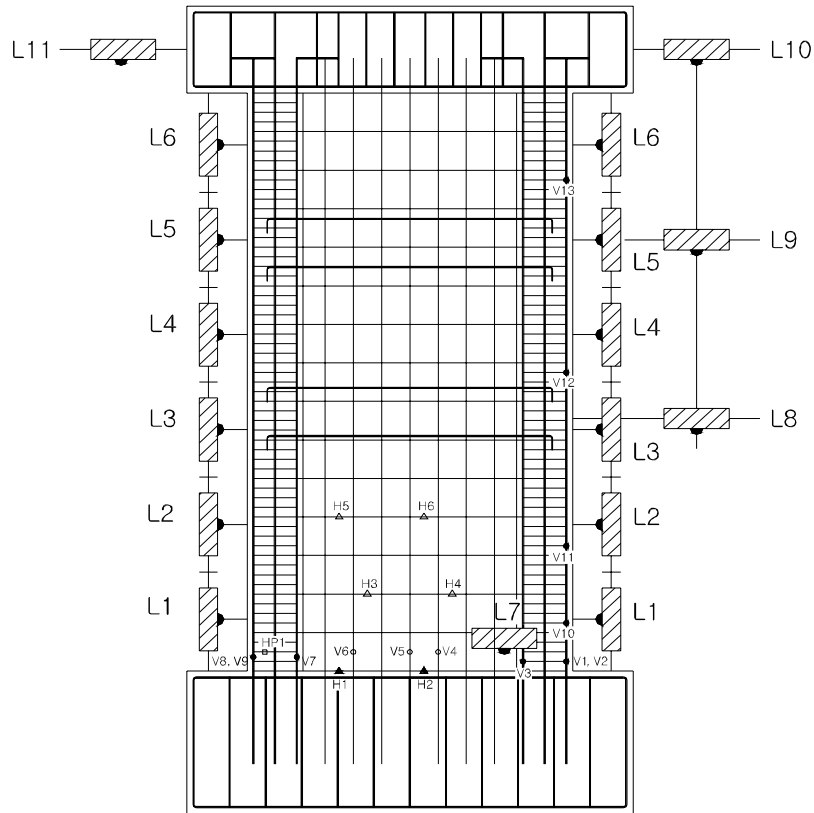Fig. 1 Geometry and reinforcement details(section A-A) of wall specimens (unit : mm)
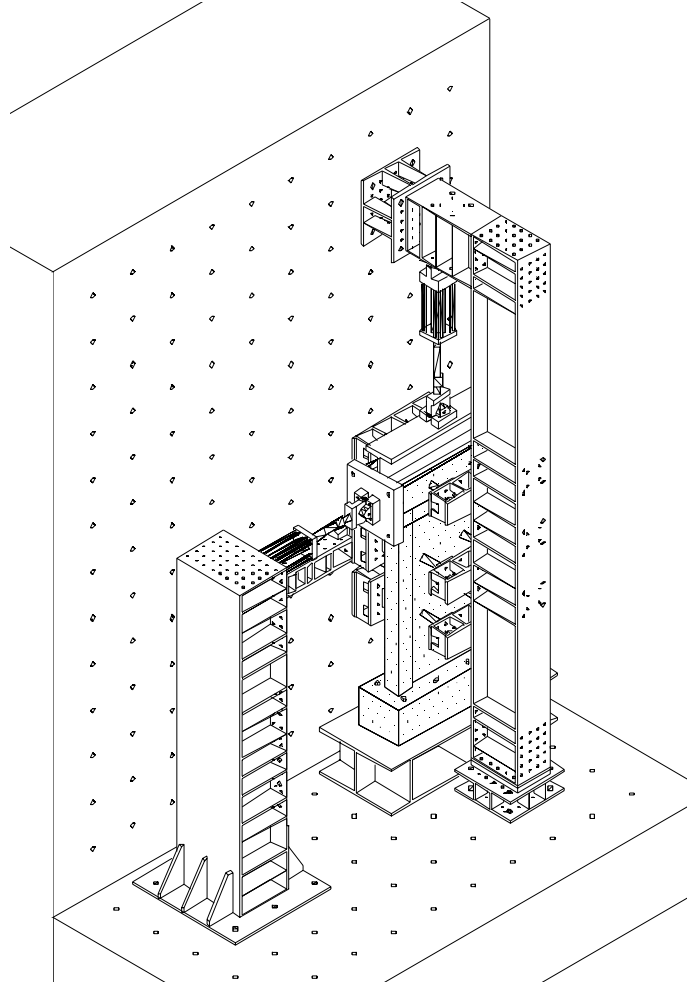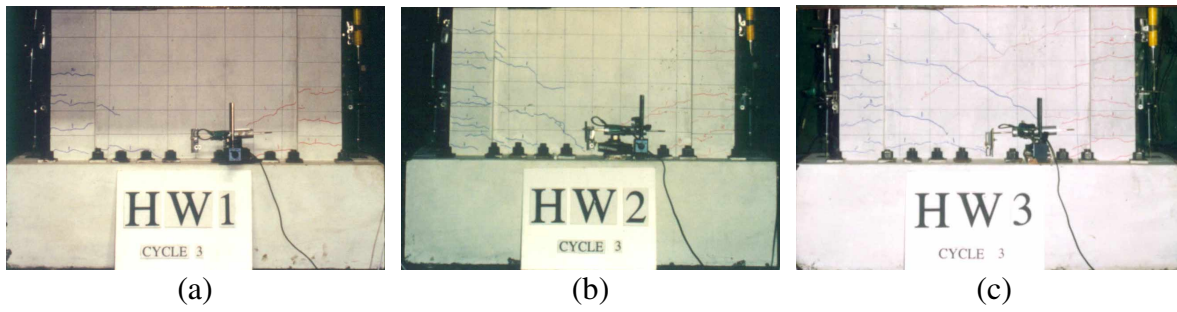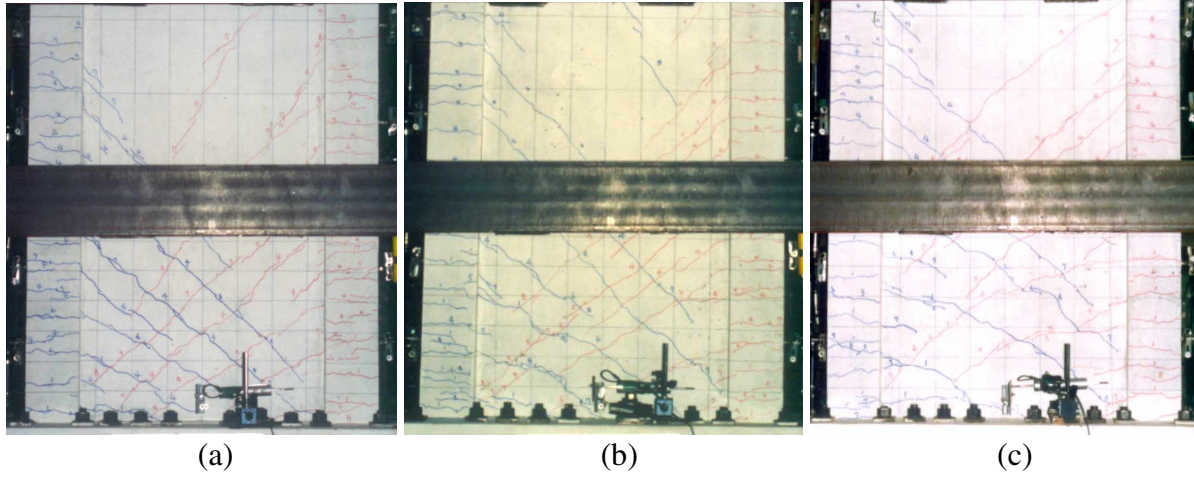
Fig. 2 Test setup
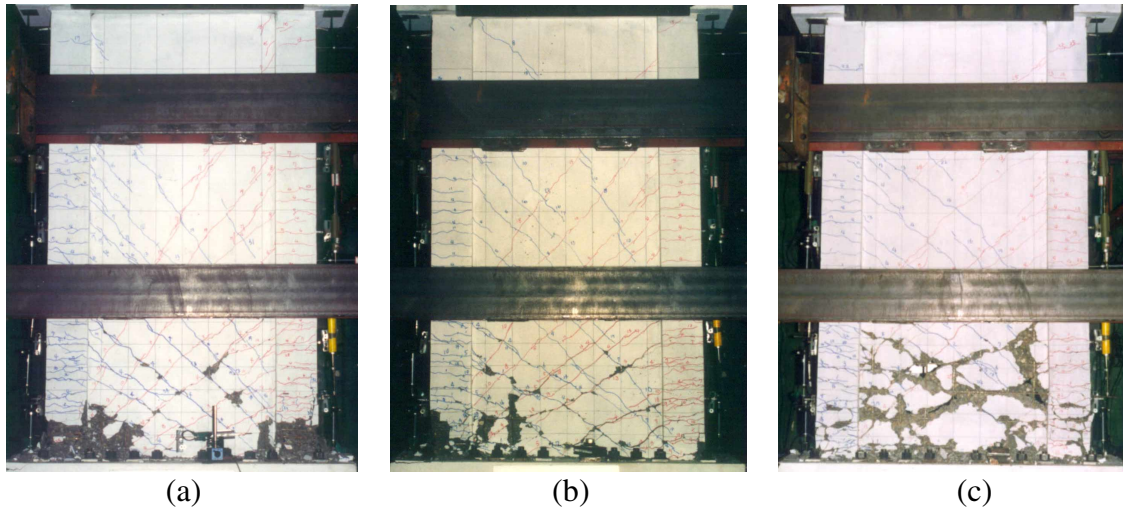
Fig. 3 Instrumentation arrangement

(a)   (b)   (c)

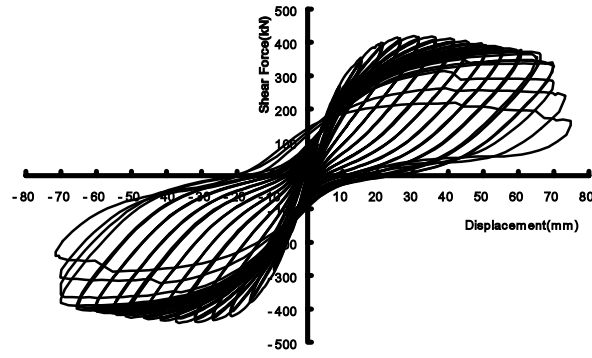(a) HW1; (b) HW2; and (c) HW3

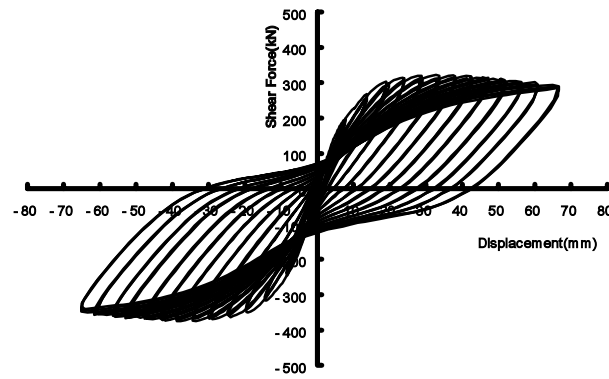Fig. 4 Cracking pattern at the yielding stage

(a)   (b)   (c)

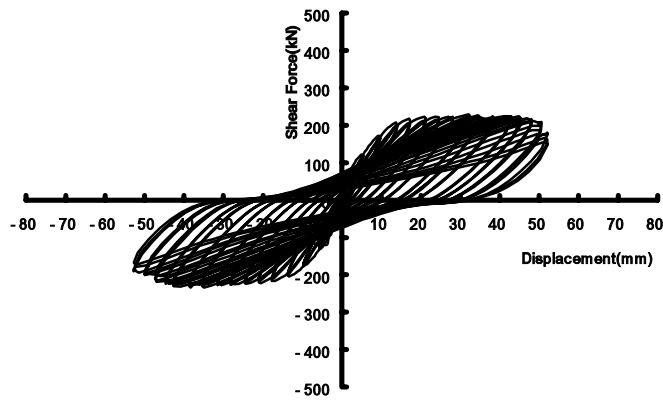(a) HW1; (b) HW2; and (c) HW3

Fig. 5 Cracking pattern at the ductility ratio of 3

(a)   (b)   (c)

(a) HW1; (b) HW2; and (c) HW3

Fig. 6 Failure Modes

(a)

(b)

(c)

(a) HW1; (b) HW2; and (c) HW3
Fig. 7 Horizontal load versus top horizontal displacement
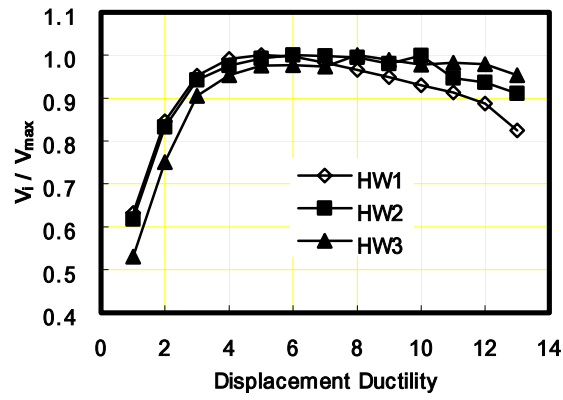
Fig. 8 Degradation of strength(V_i/V_{max})
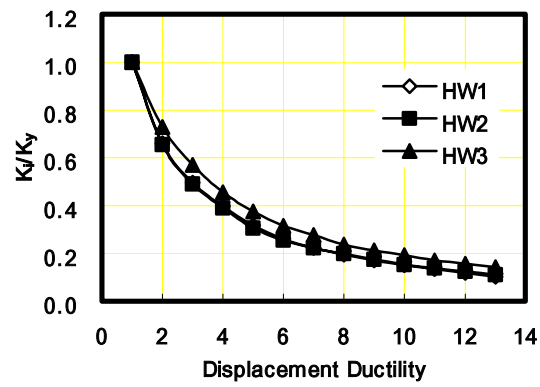
Fig. 9 Degradation of stiffness(k_i/k_y)
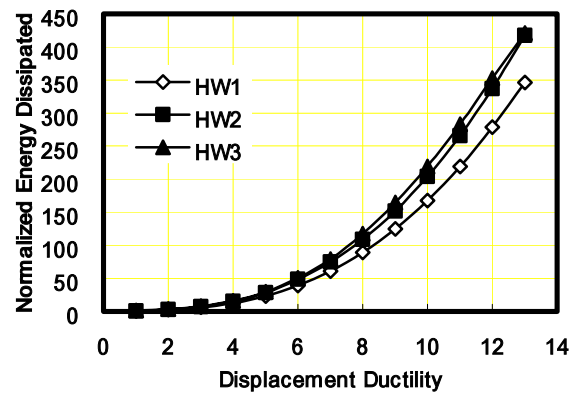
Fig. 10 Normalized energy dissipated
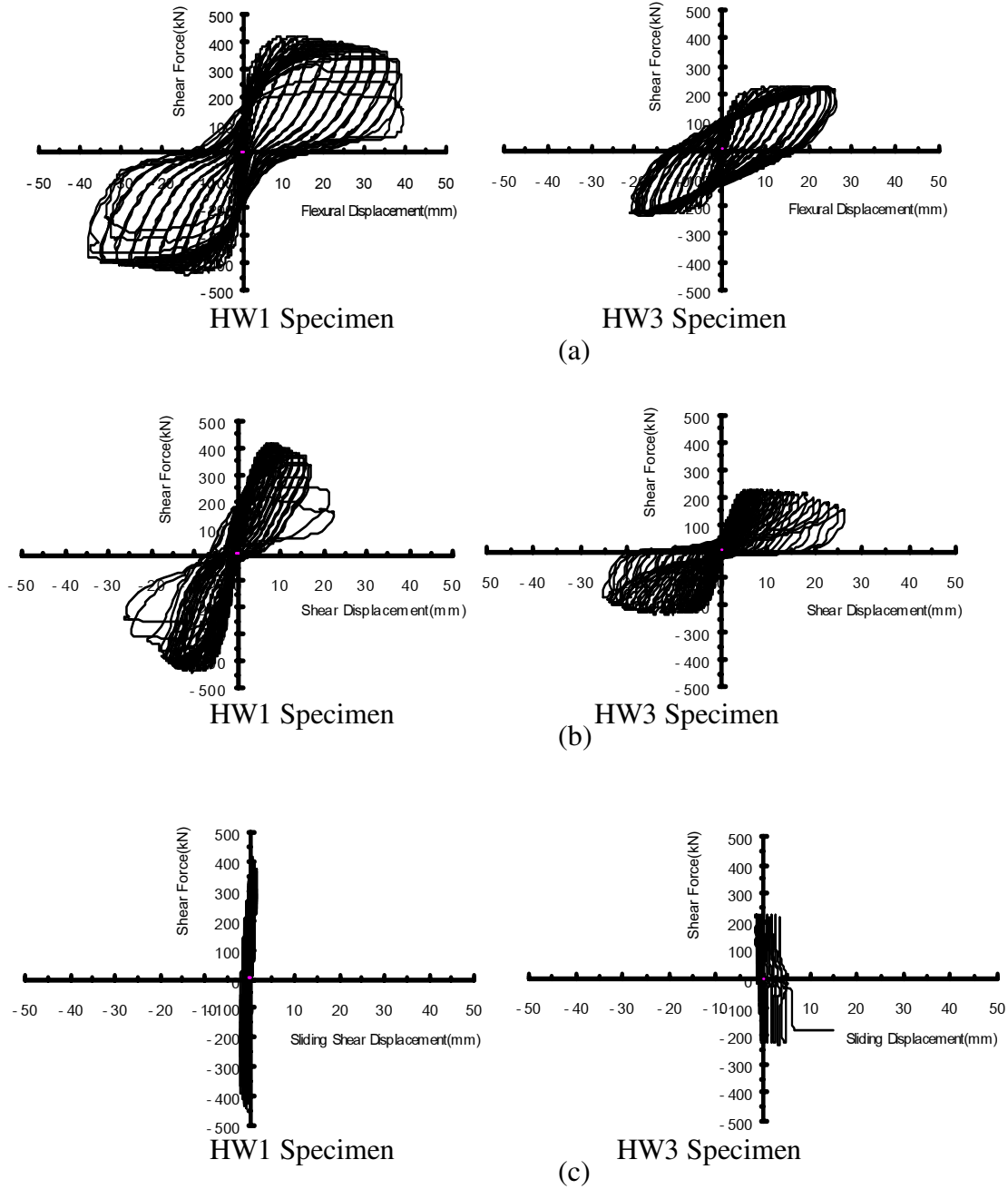
(a) shear force versus flexural displacement; (b) shear force versus shear displacement;
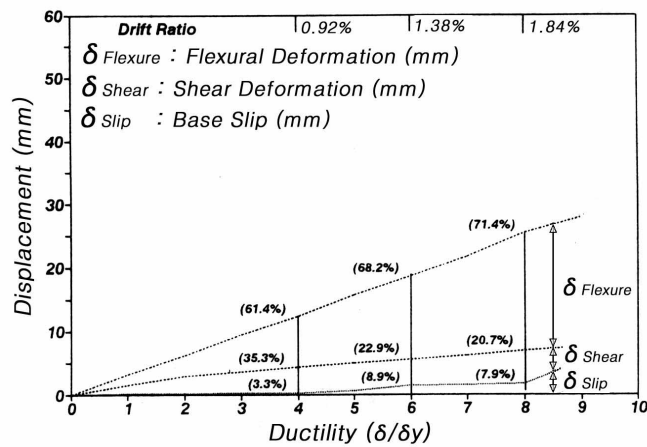and (c) shear force versus sliding displacement
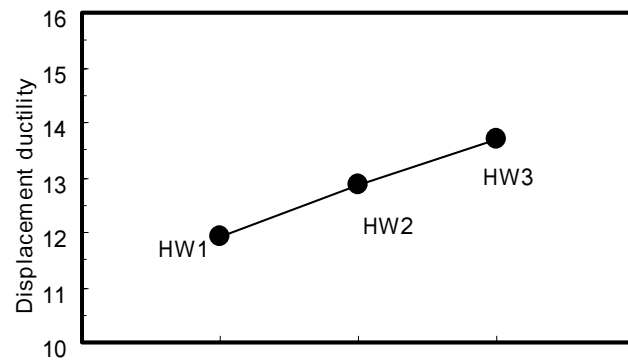Fig. 11 Hysteresis loops for HW1 and HW3 specimens.
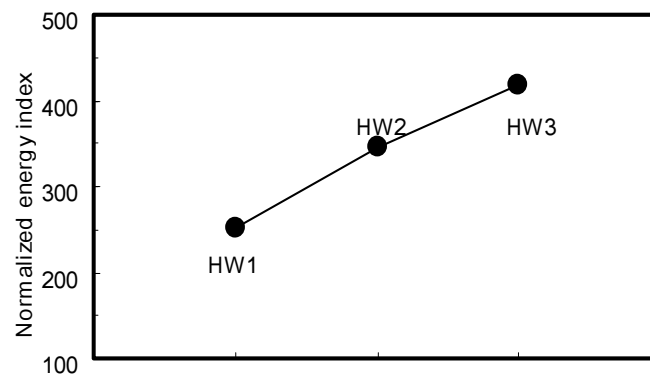
(a)

(b)

(c)
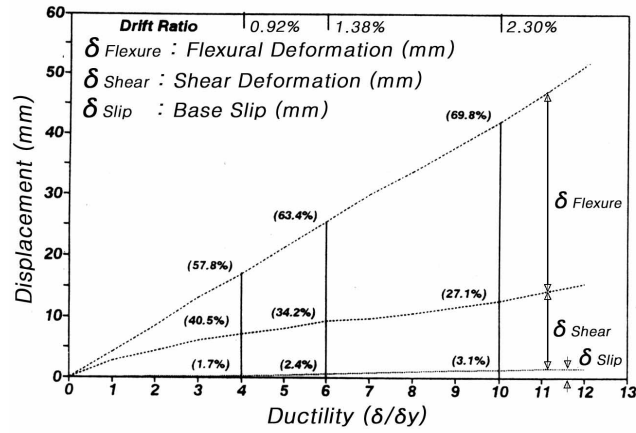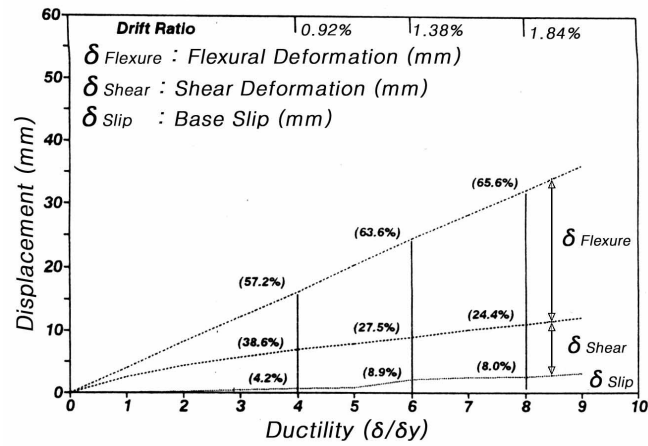
(a) HW1; (b) HW2; and (c) HW3
Fig. 12 Displacement components

(a)

(b)

(a) ductility; and (b) damage index
Fig. 13 Damage index of walls.